RSC Advances

PAPER

Cite this: *RSC Adv.*, 2019, **9**, 30581

Iron phosphide nanoparticles as a pH-responsive T_1 contrast agent for magnetic resonance tumor imaging†

Yuan Qiu,‡[a] Weiwen Lin,‡[b] Lili Wang,‡[b] Rui Liu,[a] Jiangao Xie,[b] Xin Chen,[a] Feifei Yang,[a] Guoming Huang *[a] and Huanghao Yang *[c]

Received 30th August 2019
Accepted 17th September 2019

DOI: 10.1039/c9ra06886d

rsc.li/rsc-advances

In this work, the potential of FeP nanoparticles as a pH-responsive T_1 contrast agent was investigated. The FeP nanoparticles have good biocompatibility and can significantly amplify T_1 magnetic resonance signals in response to the acidic microenvironment of solid tumors, holding great promise in serving as an acid-activatable T_1 contrast agent for tumor imaging.

Magnetic resonance imaging (MRI) is currently one of the most powerful medical imaging techniques due to its noninvasive character, deep tissue penetration, and ability to provide images with excellent anatomical details.[1–3] MRI contrast agents are a group of contrast media that can improve the accuracy and specificity of MRI.[4–6] In general, MRI contrast agents can be divided into T_1 positive contrast agents and T_2 negative contrast agents according to the relaxation processes. T_1 contrast agents shorten the longitudinal relaxation time of water protons, resulting in a brighter signal, while T_2 contrast agents reduce the transverse relaxation time, leading to a darker signal.[7,8] Nanomaterials containing paramagnetic metal ions (*e.g.*, Gd^{3+}, Mn^{2+}, and Fe^{3+}) have been widely used as T_1 MRI contrast agents.[9–14] On the other hand, magnetic nanoparticles with high saturation magnetization are the most commonly used as T_2 contrast agents because they can generate a local magnetic field in the presence of the external magnetic field to accelerate the dephasing of surrounding water protons.[15–17]

The exploitation of highly specific and sensitive imaging contrast agents is of great importance for precise disease diagnosis.[18] Activatable imaging contrast agents that can respond to biological stimulis (*e.g.*, pH, redox potential, and enzyme) to produce contrast signals, have emerged as the next generation of molecular imaging probes.[19–22] They can minimize the signal from nontarget background, therefore greatly improve the target-to-background ratio. Conventional T_1 contrast agents such as Gd_2O_3 nanoparticles and MnO nanoparticles have been demonstrated that can afford effective T_1 shortening effect to improve the visibility. However, these contrast agents continuously emit signals are "always on", which fail to response to pathological parameters and hence lack in specificity and sensitivity. Activatable MRI contrast agents that only generate signals in response to a certain stimuli (*e.g.*, physiological difference in pH in tumor microenvironment) thus are highly desirable, because they not only greatly enhance the specificity and sensitivity of disease diagnosis, but also potentially allow MRI to monitor biological processes.[23–25] Herein, we report a novel pH-activatable T_1 contrast agent based on FeP nanoparticles. We found that the as-synthesized FeP nanoparticles can respond to the acidic microenvironment of solid tumor to produce significant T_1 contrast enhancement by releasing paramagnetic Fe ions. Furthermore, both *in vitro* and *in vivo* investigations indicate that the FeP nanoparticles have good biocompatibility that show no obvious cytotoxicity and harmful effects. Therefore, the FeP nanoparticles can potentially serve as an acid-responsive T_1 MRI contrast agent for tumor imaging.

Results and discussion

We first synthesized the FeP nanoparticles by a thermal decomposition method using $Fe(acac)_3$ as the iron precursor and trioctylphosphine (TOP) as the phosphide precursor. To render the as-synthesized FeP nanoparticles water-soluble and biocompatible, we then modified these nanoparticles with poly(ethylene glycol) (PEG). Transmission electron microscopy (TEM) image shows that the FeP nanoparticles have a small size with the average particle size of 9.60 ± 1.73 nm (Fig. 1a). High-resolution TEM (HRTEM) image clearly reveals the lattice spacing of FeP nanoparticles, indicating the crystalline nature of the nanoparticles (Fig. 1a inset). The measured lattice spacing is about 0.27 nm, corresponding to the (011) plane of

[a]*College of Biological Science and Engineering, Fuzhou University, Fuzhou 350116, P. R. China. E-mail: gmhuang@fzu.edu.cn*

[b]*Department of Diagnostic Radiology, Union Hospital, Fujian Medical University, Fuzhou 350001, P. R. China*

[c]*MOE Key Laboratory for Analytical Science of Food Safety and Biology, Fujian Provincial Key Laboratory of Analysis and Detection Technology for Food Safety, College of Chemistry, Fuzhou University, Fuzhou 350116, P. R. China. E-mail: hhyang@fzu.edu.cn*

† Electronic supplementary information (ESI) available: Experimental and theoretical details, Fig. S1–S9. See DOI: 10.1039/c9ra06886d

‡ These authors contributed equally to this work.

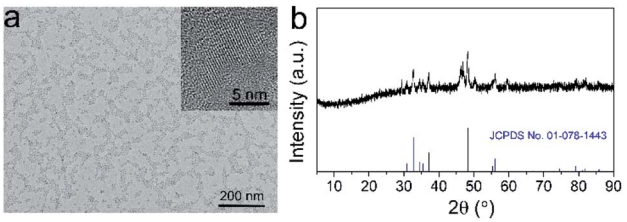

Fig. 1 (a) TEM image (inset: HRTEM image) and (b) XRD pattern of FeP nanoparticles.

FeP. TEM-associated energy-dispersive X-ray spectroscopy (EDS) shows typical peaks of Fe and P (Fig. S1†). Moreover, X-ray diffraction (XRD) pattern confirms that the crystal phase of the as-synthesized nanoparticles is FeP (JCPDS no. 01-078-1443). These results suggest that FeP nanoparticles have been successfully synthesized. Fourier transform infrared (FTIR) spectrum presents the typical asymmetric and symmetric $-CH_2-$ stretching bands (2918 cm^{-1} and 2850 cm^{-1}) and –C–O–C group vibrations (1000–1500 cm^{-1}), confirming the successful modification of PEG (Fig. S2†).[26] Dynamic light scattering (DLS) measurements were used to investigate the hydrodynamic diameter of FeP nanoparticles (Fig. S3†). The hydrodynamic diameters of FeP nanoparticles in various solutions including water, phosphate buffered saline (PBS), and fetal bovine serum (FBS) are in the range of 20–25 nm. Furthermore, these hydrodynamic diameters have no obvious change over at least 7 days, indicating the good stability of FeP nanoparticles.

To investigate the pH-responsive T_1 MRI performance of FeP nanoparticles, we dispersed the nanoparticles in buffers with different pH values and conducted the measurements. We first collected the T_1-weighted phantom images (Fig. 2a). Significant brighten signals can be detected when FeP nanoparticles are dispersed in acidic buffers (pH 5.0 and pH 6.0), suggesting that FeP nanoparticles generate T_1 contrast enhancement at acidic conditions. In contrast, no obvious brighten signals are measured at pH 7.4, demonstrating that FeP nanoparticles have little contrast enhancement effect under neutral conditions. We then measured the longitudinal relaxivity (r_1) values of FeP nanoparticles (Fig. 2b). FeP nanoparticles have a relatively low r_1 value (~0.2 mM^{-1} s^{-1}) at pH 7.4, and the value show little change over time, suggesting FeP nanoparticles have little T_1 shortening effect under neutral conditions. In contrast, a gradual enhancement in r_1 values can be observed when FeP nanoparticles are in acidic buffers. For example, the r_1 value of FeP nanoparticles increases to 4.6 ± 0.2 mM^{-1} s^{-1} for pH 5.0 at 24 h. This value is close to that of commercial Gd-based MRI contrast agents such as Gd-DTPA and Gd-DOTA (4–5 mM^{-1} s^{-1} at 0.5 T).[10,22,27] These results confirm that FeP nanoparticles can effectively shorten the T_1 relaxation time of the surrounding water protons at acidic environments. To investigate this pH-responsive behavior of FeP nanoparticles, we further measured the release of Fe ions from FeP nanoparticles under different pH conditions by ICP-MS (Fig. S4†). FeP nanoparticles show very little release of Fe ions at pH 7.4 buffer. However, a significant increase in the release of Fe ions can be detected when FeP nanoparticles are in acidic environments. Paramagnetic Fe ions have the ability to shorten the T_1 relaxation time of the water protons because of their high magnetic moment and long electron spin relaxation time. The pH-dependent release property makes FeP nanoparticles to be potential contrast agents for acid-triggered MRI. We further investigated the pH-responsive imaging ability of FeP nanoparticles in cells. MCF-7 cells were incubated with FeP nanoparticles and then were harvested at different time points for imaging. T_1-weighted images show that the T_1 signals of MCF-7 cells gradually enhance with the increase of incubation time (Fig. 2c). Cells can uptake nanomaterials *via* endocytosis and the nanomaterials are trapped in endosomes and lysosomes.[28] The acidic environment of endosomes/lysosomes trigger FeP nanoparticles to release Fe ions, thus resulting in the T_1 signal enhancement inside the cells.

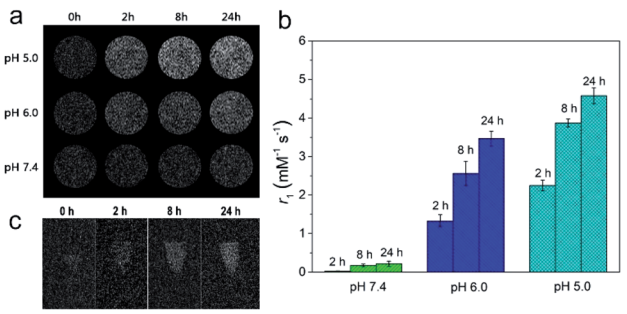

Fig. 2 (a) T_1-weighted phantom images of FeP nanoparticles (0.4 mM [Fe]) under different pH conditions. (b) r_1 values collected at different time points of FeP nanoparticles in different pH buffers. (c) T_1-weighted images of MCF-7 cells after incubating with FeP nanoparticles for different time points.

We then investigated the *in vivo* acid-responsive MRI performance of FeP nanoparticles using MCF-7 tumor bearing mice as models. The biodistribution analysis confirms that FeP nanoparticles can effectively accumulate in tumor *via* enhanced permeability and retention (EPR) effect (Fig. S5†). T_1-weighted images of the mice were collected before and after the injection of FeP nanoparticles at different time points. Gradual brightening signals can be observed in tumor areas after the injection of FeP nanoparticles (Fig. 3a). To further quantify the contrast enhancement, we calculated the signal-to-noise ratio (SNR) in tumor region, and defined the contrast enhancement as the change of SNR, where $\Delta SNR = (SNR_{post} - SNR_{pre})/SNR_{pre}$. The measured ΔSNR values are 56.0 ± 23.8%, 82.7 ± 13.6%, 26.5 ± 8.6% at 2 h, 8 h, 24 h after the injection, respectively (Fig. 3b). This time-dependent T_1 signal change confirms that FeP nanoparticles can respond to acidic microenvironment of tumor, leading to the shortening effect of T_1 relaxation in tumor area.

Biocompatibility is the key factor for a nanoparticle for biomedical applications. To investigate the biocompatibility of FeP nanoparticles, we first assessed the cytotoxicity of by tetrazolium-based colorimetric assay (MTT assay). FeP nanoparticles show no significant cytotoxicity on both MCF-7 and L02 cells after being incubated with these cells for 24 h,

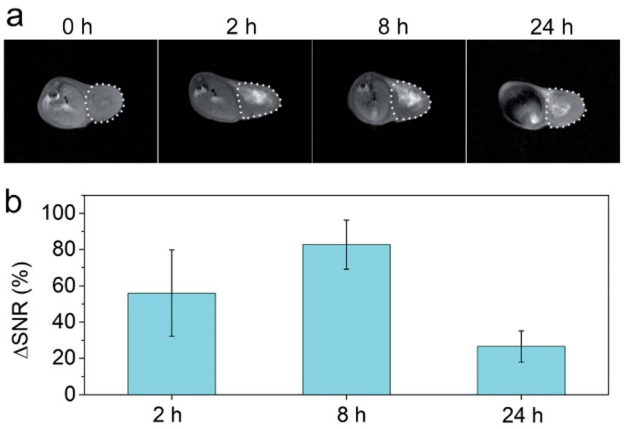

Fig. 3 (a) T_1-weighted images and (b) corresponding quantificational analyses of signal-to-noise changes (ΔSNR) of mice at different time points after the injection of FeP nanoparticles ($n = 3$). The regions of tumor are indicated by dashed lines.

suggesting the little cytotoxicity of FeP nanoparticles (Fig. S6†). We then evaluated the *in vivo* toxicity of FeP nanoparticles in mice. The mice were injected with FeP nanoparticles, and after 14 days, haematoxylin and eosin (H&E) stained histological images of major organs were collected to study the systemic toxicity of FeP nanoparticles. All major organs including heart, liver, spleen, lung, and kidney, maintain their typical tissue structures and exhibit no appreciable organ damage or inflammatory lesion, indicating the long-term safety of FeP nanoparticles (Fig. 4a). Moreover, blood biochemistry and hematology analyses of the mice were also performed (Fig. 4b). Various serum biochemistry parameters including aspartate transaminase (ALT), alanine aminotransferase (AST), blood urea nitrogen (BUN), and creatinine (CRE) maintain at similar

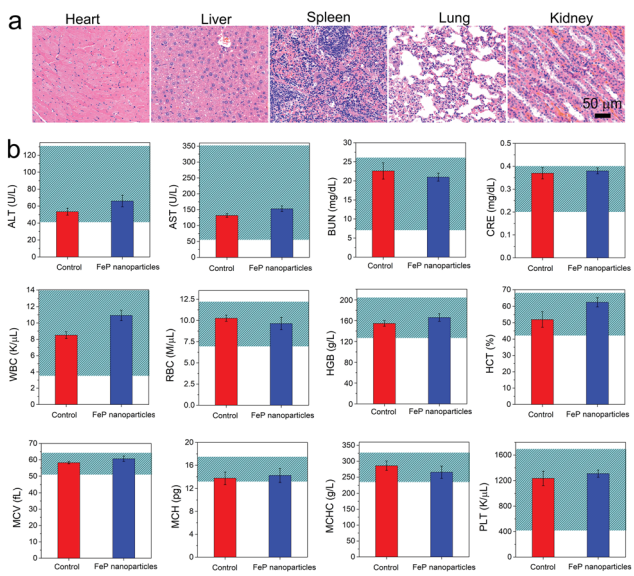

Fig. 4 (a) H&E stained histological images and (b) blood biochemistry and hematology analyses ($n = 5$) of the mice collected at 14 days after the injection of FeP nanoparticles.

levels as the controls and all fall within the normal reference intervals, suggesting that the injection of FeP nanoparticles does not affect the liver and kidney functions of mice. The hematology indices including white blood cells (WBC), red blood cells (RBC), hemoglobin (HGB), hematocrit (HCT), mean corpuscular volume (MCV), mean corpuscular hemoglobin (MCH), mean corpuscular hemoglobin concentration (MCHC), and platelet count (PLT) also show no significant physiological difference comparing to the control group and maintain at normal levels, further confirming the long-term biosafety of FeP nanoparticles.

Conclusions

In summary, we have synthesized successfully FeP nanoparticles *via* a simple method. The as-prepared FeP nanoparticles exhibit pH-dependent MRI performance that the T_1 contrast signals could be significantly amplified in acidic environments. The *in vivo* imaging studies show that FeP nanoparticles can respond to the acidic microenvironment to generate significant T_1 contrast enhancement in tumor region. Moreover, the MTT assay indicates that FeP nanoparticles show very little cytotoxicity. The histological and hematological analyses confirm the *in vivo* long-term biosafety of FeP nanoparticles. We believe that this acid-responsive T_1 MRI contrast agent should have great potential in precise diagnosis of tumor.

Conflicts of interest

There are no conflicts of interest to declare.

Acknowledgements

This work was supported by the National Natural Science Foundation of China (Grant No. 81501461, U1505221, and 21635002); Natural Science Foundation of Fujian Province (Grant No. 2018J01896, 2017J05131, and 2017J01199); Joint Funds for the Innovation of Science and Technology, Fujian Province (Grant No. 2017Y9041); and Program for Changjiang Scholars and Innovative Research Team in University (Grant No. IRT15R11); Scientific Foundation of Fujian Provincial Health Commission (Grant No. 2018-ZQN-37 and 2016-1-44).

Notes and references

1 R. Weissleder and M. J. Pittet, *Nature*, 2008, **452**, 580–589.
2 B. R. Smith and S. S. Gambhir, *Chem. Rev.*, 2017, **117**, 901–986.
3 G. Huang, C.-H. Lu and H.-H. Yang, in *Novel Nanomaterials for Biomedical, Environmental and Energy Applications*, ed. X. Wang and X. Chen, Elsevier, 2019, ch. 3, pp. 89–109, DOI: 10.1016/b978-0-12-814497-8.00003-5.
4 Z. Zhou, L. Yang, J. Gao and X. Chen, *Adv. Mater.*, 2019, **31**, e1804567.
5 Z. Zhou, R. Bai, J. Munasinghe, Z. Shen, L. Nie and X. Chen, *ACS Nano*, 2017, **11**, 5227–5232.

6 G. Huang, H. Li, J. Chen, Z. Zhao, L. Yang, X. Chi, Z. Chen, X. Wang and J. Gao, *Nanoscale*, 2014, **6**, 10404–10412.
7 H. B. Na, I. C. Song and T. Hyeon, *Adv. Mater.*, 2009, **21**, 2133–2148.
8 D. Ni, W. Bu, E. B. Ehlerding, W. Cai and J. Shi, *Chem. Soc. Rev.*, 2017, **46**, 7438–7468.
9 H. B. Na and T. Hyeon, *J. Mater. Chem.*, 2009, **19**, 6267.
10 T. Guo, Y. Lin, Z. Li, S. Chen, G. Huang, H. Lin, J. Wang, G. Liu and H. H. Yang, *Nanoscale*, 2017, **9**, 56–61.
11 T. Guo, Y. Lin, G. Jin, R. Weng, J. Song, X. Liu, G. Huang, L. Hou and H. Yang, *Chem. Commun.*, 2019, **55**, 850–853.
12 Z. Zhou, L. Wang, X. Chi, J. Bao, L. Yang, W. Zhao, Z. Chen, X. Wang, X. Chen and J. Gao, *ACS Nano*, 2013, **7**, 3287–3296.
13 Z. Zhou, C. Wu, H. Liu, X. Zhu, Z. Zhao, L. Wang, Y. Xu, H. Ai and J. Gao, *ACS Nano*, 2015, **9**, 3012–3022.
14 R. Wei, Z. Cai, B. W. Ren, A. Li, H. Lin, K. Zhang, H. Chen, H. Shan, H. Ai and J. Gao, *Chem. Mater.*, 2018, **30**, 7950–7961.
15 G. Huang, J. Hu, H. Zhang, Z. Zhou, X. Chi and J. Gao, *Nanoscale*, 2014, **6**, 726–730.
16 K. L. Zhang, J. Zhou, H. Zhou, Y. Wu, R. Liu, L. L. Wang, W. W. Lin, G. Huang and H. H. Yang, *ACS Appl. Mater. Interfaces*, 2017, **9**, 30502–30509.
17 Z. Zhao, Z. Zhou, J. Bao, Z. Wang, J. Hu, X. Chi, K. Ni, R. Wang, X. Chen, Z. Chen and J. Gao, *Nat. Commun.*, 2013, **4**, 2266.
18 H. Chen, Z. Gu, H. An, C. Chen, J. Chen, R. Cui, S. Chen, W. Chen, X. Chen, X. Chen, Z. Chen, B. Ding, Q. Dong, Q. Fan, T. Fu, D. Hou, Q. Jiang, H. Ke, X. Jiang, G. Liu, S. Li, T. Li, Z. Liu, G. Nie, M. Ovais, D. Pang, N. Qiu, Y. Shen, H. Tian, C. Wang, H. Wang, Z. Wang, H. Xu, J.-F. Xu, X. Yang, S. Zhu, X. Zheng, X. Zhang, Y. Zhao, W. Tan, X. Zhang and Y. Zhao, *Sci. China: Chem.*, 2018, **61**, 1503–1552.
19 J. Li, F. Cheng, H. Huang, L. Li and J.-J. Zhu, *Chem. Soc. Rev.*, 2015, **44**, 7855–7880.
20 H. Kobayashi and P. L. Choyke, *Acc. Chem. Res.*, 2011, **44**, 83–90.
21 G. Huang, K.-L. Zhang, S. Chen, S.-H. Li, L.-L. Wang, L.-P. Wang, R. Liu, J. Gao and H.-H. Yang, *J. Mater. Chem. B*, 2017, **5**, 3629–3633.
22 G. Huang, R. Liu, Y. Hu, S.-H. Li, Y. Wu, Y. Qiu, J. Li and H.-H. Yang, *Sci. China: Chem.*, 2018, **61**, 806–811.
23 G. L. Davies, I. Kramberger and J. J. Davis, *Chem. Commun.*, 2013, **49**, 9704–9721.
24 P. Mi, D. Kokuryo, H. Cabral, H. Wu, Y. Terada, T. Saga, I. Aoki, N. Nishiyama and K. Kataoka, *Nat. Nanotechnol.*, 2016, **11**, 724–730.
25 J. Wahsner, E. M. Gale, A. Rodriguez-Rodriguez and P. Caravan, *Chem. Rev.*, 2019, **119**, 957–1057.
26 X. Qiu, X. Zhu, X. Su, M. Xu, W. Yuan, Q. Liu, M. Xue, Y. Liu, W. Feng and F. Li, *Adv. Sci.*, 2019, **6**, 1801834.
27 L. Wang, X. Zhu, X. Tang, C. Wu, Z. Zhou, C. Sun, S. L. Deng, H. Ai and J. Gao, *Chem. Commun.*, 2015, **51**, 4390–4393.
28 F. Zhao, Y. Zhao, Y. Liu, X. Chang, C. Chen and Y. Zhao, *Small*, 2011, **7**, 1322–1337.